The Supplement of
Carbon Balance of an Afforested Wasteland: A Case Study to Quantify Emission Offset Units

Suvi Orttenvuori[1], Tuomas Laurila[1], Leif Backman[1], Esko Karvinen[1], Elina Nieminen[1], Henriikka Vekuri[1], Olli Nevalainen[1], Juuso Rainne[1], Jari Liski[1], Liisa Kulmala[1]

[1]Finnish Meteorological Institute

1 Soil preparation and climate

The soil parental matter was clay with a carbon content of app. 1.4%. The carbon pool in the new organic layer levelled on top of the clay was estimated to be app. 17.4 kg C m^{-2}. The estimation was based on an approximation that the topsoil was app. 30 cm deep and it composed of equal shares of bark, woody materials and composted sludge. Furthermore, we utilized the measured densities and the losses of ignition for each material. The acid (A) hydrolyzable, water (W) soluble, ethanol (E) soluble, neither soluble or hydrolyzable (N), and humus (H) fractions of the different components were estimated based on literature and personal discussion (Table 1).

The 30-year mean annual precipitation and temperature are 614 mm and 4.7 °C, respectively, at Lahti Laune weather station situated 29 km from the site (Jokinen et al. (2021)).

Table 1: Estimated carbon pools, AWENH values, and diameters for the three different substartes mixed on top of the clay soil before planting and sowing of the vegetation.

Parameter (unit)	*Bark*	*Wood*	*Sludge*
C pool (kg m^{-2})	6.3	4.9	6.4
A (%)	48	67	62
W (%)	1.9	1.8	4.9
E (%)	7.8	0.3	2.3
N (%)	43	31	31
H (%)	0	0	0
Diameter (cm)	0.5–5	2–4	0
AWEN reference	[1]	[2]	[3]

[1] Bark according to personal communication with Aleksi Lehtonen, 2020
[2] Spruce wood according to personal communication with Aleksi Lehtonen, 2020
[3] Composted sludge according to Heikkinen et al. (2021)

2 Measurement setup

The micrometeorological eddy covariance (EC) instrumentation included an enclosed IR gas analyser (LI-7200, LI-COR Biosciences Inc., Lincoln, Nebraska, USA) to measure CO_2 mixing ratio and a ultrasonic anemometer (uSonic-3 Scientific, METEK GmbH, Elmshorn, Germany) to measure the wind speed components and sonic temperature. The measurement height was 2.2 m and the the signals were recorded at 10 Hz frequency. Since the measurement area covers only 1 ha, the EC tower was placed on the eastern

side of the field, and EC data from the eastern wind sector were discarded (Fig. 1).

Figure 1: Measurement site captured by drone on 1 September 2020. The location of the eddy covariance tower (red asterisk), the cardinal directions (white), approved wind directions for EC data (white), and the three sample plots (yellow), each 100 m^2 in size, are illustrated in the figure.

A wide range of supporting meteorological measurements were conducted. Air temperature was recorded with Pt100 sensor (Nokeval Oy, Nokia, Finland) and with HMP110 probe (Humicap, Vaisala Oyj, Vantaa, Finland) alongside relative humidity. The shortwave global radiation and the reflected solar radiation were measured with two pyranometers (CMP11, Kipp & Zonen B.V., Delft, the Netherlands). Photosynthetically active radiation was recorded with PQS PAR sensor (Kipp & Zonen, OTT HydroMet B.V., Delft, Netherlands). Net radiometer (NR Lite2, Kipp & Zonen) sensor was used to determine the net radiation. These measurements were recorded at 1.3 m height. The soil temperature profiles were captured on the surface and at the depths of 5 and 30 cm (Pt100 IKES sensors, Nokeval Oy). Soil moisture was captured at depths of 10 and 30 cm (ML3 ThetaProbe sensors, Delta-T Devices Ltd., Cambridge, UK). Precipitation was monitored by a weighing rain gauge (Pluvio2, OTT HydroMet GmbH, Kempten, Germany) with a wind protection shield.

In addition to the EC method, manual chamber measurements of carbon fluxes were performed during 2021–2022. Systematic chamber measurements were performed with an opaque static aluminium chamber (area: 0.36 m^2, height: 0.2 m) seven times on six different chamber base frames that were installed on the study site, two in each of the three sample plots (Fig. 1). The CO_2 concentrations were measured with a gas analyser (LI-840A, LI-COR Biosciences Inc.). Measurements of soil temperature (Pt100 IKES sensors, Nokeval Oy), soil moisture (ML3 ThetaProbe sensors, Delta-T Devices Ltd.), and air temperature and humidity (BME280, Bosch Sensortec GmbH, Germany) were conducted simultaneously with the chamber measurements.

3 Flux processing and gapfilling

We used a low measurement height (2.2 m) due to the limited size of the target area. The EC tower was placed on the eastern side of the plot and CO_2 flux data from wind directions from 9° to 176° were excluded. To ensure turbulent conditions, we only accepted observations when wind speed was above 1.2 m s^{-1} and friction velocity exceeded 0.1 m s^{-1}. In total we have 11083 half-hourly flux observations from the measurement period from 14:00 23 Jun 2020 to 6:30 29 Jun 2022. The storage flux was calculated from CO_2 concentrations at the flux measurement height with two different methods: using the average concentrations from the preceding and succeeding half-hourly periods or alternatively using

the 30-second averages in the beginning and in the end of the half-hourly flux observation. These two methods gave very similar results. The storage flux component had very small (less than 1%) effect on the CO_2 balance. This is facilitated by the low measurement height and the roughness length, which was on average 0.10 m. A concern with this kind of a rather small study area is that the flux footprint might extend beyond the borders of the target area. To estimate the CO_2 flux footprint, we used the model by Kormann & Meixner (2001). The model estimates horizontal extent of the footprint using turbulent parameters measured by the sonic anemometer. When taking an average of all accepted observations, 70% of the flux was generated within the study area, which is considered satisfactory.

The data were gap-filled using a machine learning method called extreme gradient boosting, which is based on parallel boosted decision trees. The method was applied using the 'xgboost' Python package Chen & Guestrin (2016). Hyperparameters of the model were optimized using grid search and the squared error was used as the loss function. The variables that were used to predict NEE were soil temperature at -5cm, soil moisture deficit at -10cm, leaf area index, global radiation, air temperature and relative humidity. The coefficient of determination (R^2) and the mean squared error were evaluated using 10-fold cross-validation, and the obtained values were 0.91±0.01 and 0.006±0.0007 mg CO_2 m^{-2} m^{-1}, respectively (Fig. 2).

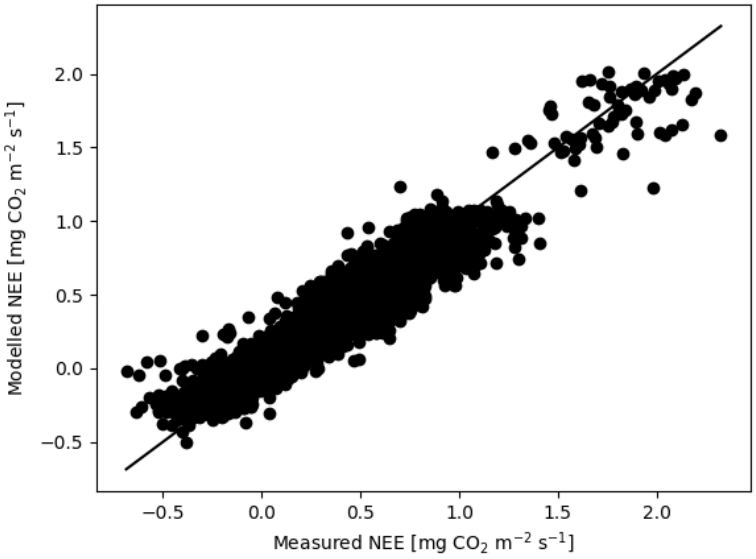

Figure 2: Comparison of modelled and measured NEE.

Momentary total ecosystem respiration (TER) was calculated from the chamber measurements for each day and closure with linear fitting function as follows,

$$TER = \frac{dc}{dt}\frac{MPV}{RTA}, \tag{1}$$

where $\frac{dc}{dt}$ is the change in CO_2 concentration over the chamber closure time (s^{-1}), M is the molar mass CO_2 (44.01 g mol^{-1}), P is air pressure (Pa), V is the chamber volume (m^3), R is the universal gas constant (8.31446 J mol^{-1} K^{-1}), T is the mean temperature in the chamber during closure (K), and A is the base area of the chamber (m^2).

4 CO_2 fluxes, energy budget and water exchange

The seasonal and diurnal variation of CO_2 fluxes was analyzed from the processed data collected during the 2-year observation period (Fig. 3). When the layer of mixed organic material was spread on the site in June 2020, the sown grass (*Festuca pratensis*) had not yet sprouted and planted tree seedlings (height app. 0.2 m) had very low projected LAI. Many of the seedlings wilted during a heatwave in June. The site carbon exchange was mostly dominated by high soil respiration, with a mean net CO_2 emission of

0.68 mg m^{-2} s^{-1} in the summer (23.6.-31.8.2020) and 0.29 mg m^{-2} s^{-1} in the autumn (1.9.-30.11.2020). As the photosynthetic production increased towards the end of the summer, a daytime net gas uptake of -0.1 mg m^{-2} s^{-1} was observed during autumn 2020. Total ecosystem respiration (TER) had a mean value of app. 0.1 mg m^{-2} s^{-1} in winter and spring 2021. Due to the easily decomposing soil and residues of grass and other litter from the 2020 growing season, CO_2 emission was strong during the night time in the summer 2021. Despite the higher LAI and favourable growth conditions, the difference between fluxes at midnight and at noon (0.5 mg m^{-2} s^{-1}) was not much more than in the previous autumn. The protracted drought during summer 2021 most likely reduced the development of vegetation. The average wintertime (1.12.-29.2.2022) gas emission was 28% lower compared to the previous winter probably due to the lower soil temperatures. In June 2022, a net CO_2 uptake developed and soil efflux remained moderate because the soil temperature had not yet reached the summer peak values.

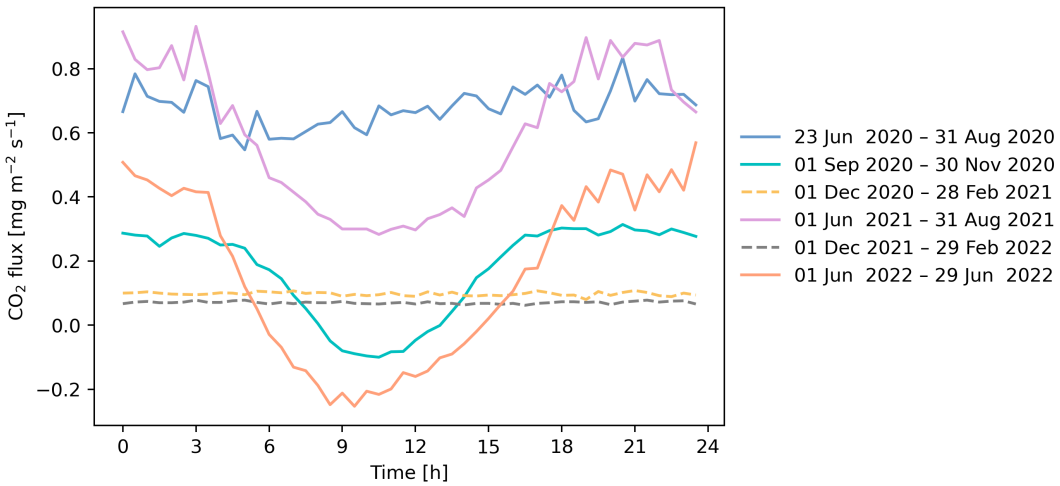

Figure 3: Mean diurnal and seasonal variation of observed CO_2 flux during 2020–2022. Negative and positive flux values indicate that the site has acted as a sink or a source of atmospheric carbon, respectively.

In the beginning of the measurement period in June 2020, the persistent heatwave induced the drying of the soil surface. In the absence of vegetation and as the recently spread layer of soil material was very porous and insulating, only the very top surface layer became notably dry. Therefore, in the absence of latent heat flux, the soil surface reached very high temperatures during the daytime. On June 27, the Bowen ratio (sensible heat flux divided by the latent heat flux) was 3.3 which is very high compared to normal vegetated surfaces with a Bowen ratio closer to 1. The Bowen ratio was calculated as the 6-hour average of the half-hourly turbulent flux values centered at noon. At daytime, the energy balance was driven by solar radiation heating the dark surface which was balanced by cooling by turbulent sensible heat flux and infrared radiation. Evaporation was only a minor component. During the heatwave in July 2021, when vegetation was more abundant, we observed Bowen ratios from 0.25 to 0.5 with evapotranspiration being the major energy balance component.

Water balance was monitored by measuring precipitation, evapotranspiration, (Fig. 4B) and soil moisture at high temporal resolution in order to understand the evapotranspiration and possibly nutrient rich soil water runoff. The observed cumulative precipitation was 474 mm from 23 June until the end of 2020, 584 mm for 2021, and 239 mm for the beginning of 2022 until 28 June 2022 while the cumulative evapotranspiration for the same time periods was 158 mm, 251 mm, and 102 mm, respectively. A dry period prevailed from May 25 to Jun 27, 2021 when cumulative precipitation amount was only 23 mm but cumulative evapotranspiration 134 mm. This resulted in very low soil moisture values (less than 0.2 m^3 m^{-3}). The following August was very wet with a precipitation sum of 163mm. In the long run, precipitation that exceeds evapotranspiration ($P - ET$ in Fig. 4C) produces runoff water which is exported from the area. In 2021, the total $P - E$ difference was 333 mm generating 3300 m^3 runoff water from the 1 ha area. During the latter half of year 2020, precipitation excess was 316 mm and during the first half of 2022, it was 137 mm.

Soil temperature (Fig. 4D) is the most important parameter for soil respiration and air temperature is very important for plant growth and plant respiration. In summer 2021, there were 33 measurement days when air temperature exceeded 25°C, with the highest air temperature of 33.3°C (July 14). Even though the freezing of soil is rare in southern parts of Finland, the soil was frozen down to 10 cm depth in December 2021 for one month. Furthermore, the frozen conditions lasted until March in the top 5 cm soil layer.

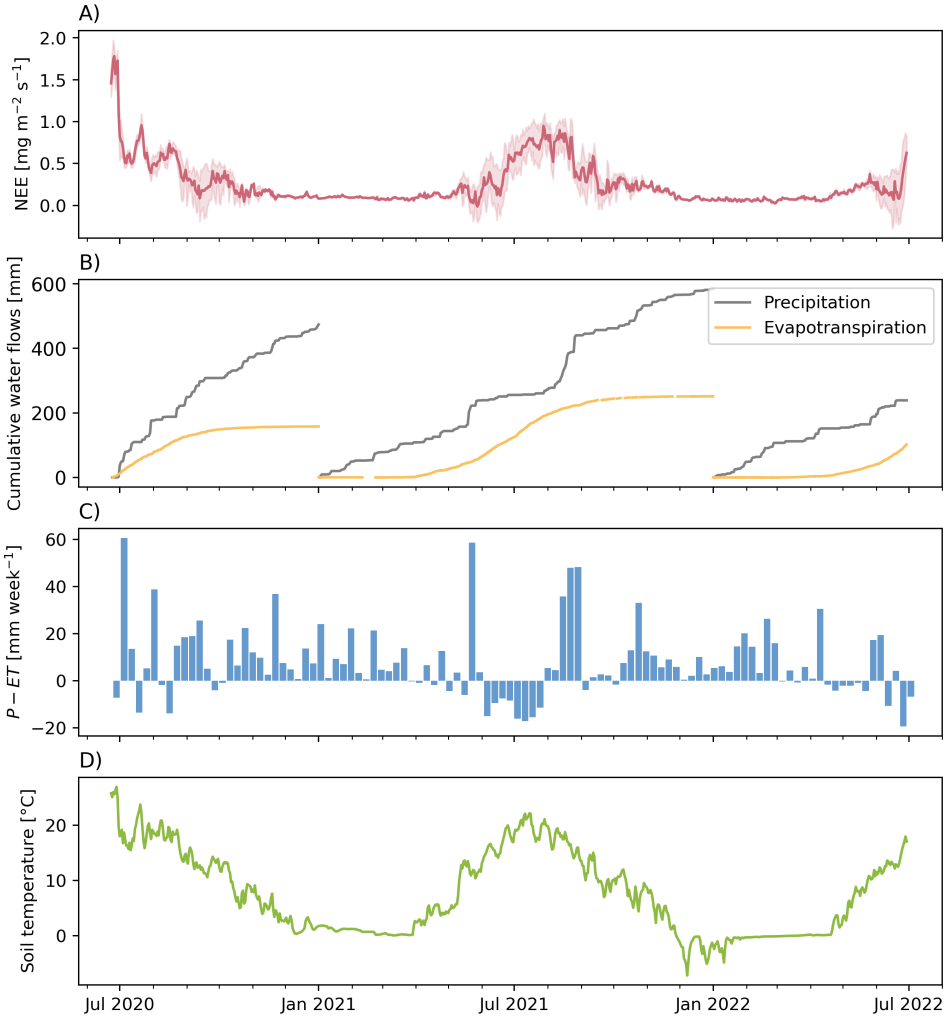

Figure 4: A time series of A) daily mean net ecosystem exchange (NEE) with shaded areas representing the 25th/75th percentiles, B) cumulative precipitation amount and evapotranspiration by micrometeorological method, C) difference between weekly sums of precipitation and evapotranspiration, and D) daily mean soil temperature (5 cm). Negative and positive NEE values indicate that the site has acted as a sink or a source of atmospheric carbon, respectively.

The CO_2 fluxes from the systematic manual opaque chamber measurements showed similar seasonal pattern wit the nocturnal EC fluxes on the site (Fig. 5). The gas fluxes were averaged separately over the three bare and three vegetated chamber measurements on each measurement day. As the EC observations and chamber measurements were taken at different times of a day, they are not directly comparable with each other due to the diurnal variation of soil temperature which strongly affects the soil respiration. However, some distinct behavior can be seen from the results. In the early summer in 2021 from May to June, both the bare and vegetated means display fluxes of similar magnitude (0.3 g m^{-2} s^{-1} and 0.7 g m^{-2} s^{-1} for May and June). During the later summer months the vegetated chambers produced higher respiration values with the maximum difference of 0.57 g m^{-2} s^{-1} between the bare and vegetated chambers on Aug 9 2021. On average, the measured fluxes were 39 % greater in the vegetated chambers than in the bare chambers. Overall, the averaged bare chamber measurements of CO_2 fluxes agreed better with the EC observations in 2021.

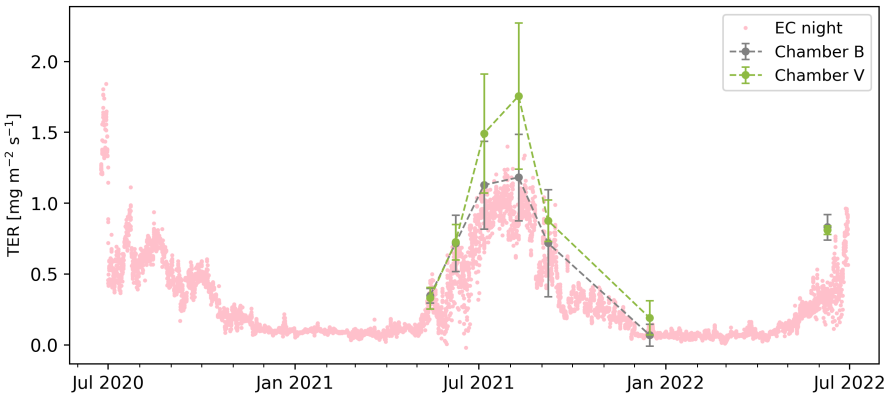

Figure 5: Ecosystem respiration compared between EC night-time (22:00-03:00) CO_2 flux observations and manual chamber measurements collected in the morning. Chamber B values are the averages of the three chambers with bare soil in May 2021 and chamber V values are the averages of the three chambers with vegetation (B=bare, V=vegetated). The error bars represent the standard deviation.

5 Vegetation

Leaf area index was measured with LAI-2200C (LI-COR Biosciences Inc.). Leaf Area Index is one-sided leaf surface area per ground surface area. On 1 September and 15 October 2020, LAI was measured on a straight line towards west (white line in Fig. 1) from the EC tower at every two meters, 22 times in total. In addition, LAI was measured 37 times in various parts of the area on 1 September 2020. On 15 October 2020, three sample plots (3×100 m^2) were established on the site and LAI was measured within these plot areas. In 2021-2022 LAI was measured along the borders of the three plot areas, on the straight line west from the EC tower, and also within the six chamber base frames.

The site was monitored also using remote sensing imagery from the Copernicus Sentinel-2 satellites during 2020-2022. Atmospherically corrected Level-2A (L2A) Sentinel-2 multispectral data were retrieved using the GEE (earthengine.google.com) cloud data platform. The scene classification band available in L2A products is used to filter away image acquisition dates during which the field is covered by snow, cloud, or cloud shadow. From the Sentinel-2 data, we calculated the green leaf area index (LAI) estimated using the ESA Sentinel Application Platform (SNAP) Biophysical Processor neural network algorithm (Weiss & Baret (2016), github.com/ollinevalainen/satellitetools). The uncertainty calculations are described in detail by Nevalainen et al. (2022).

The LAI derived from the Sentinel-2 images experienced seasonal and year-to-year variation in the study site and in a reference agricultural grain field that was located near the site (Fig. 6). In 2019, a year before the afforestation measures and the measurement campaign begun, the largest LAI values were observed in July with a monthly average LAI of 0.98 m^2 m^{-2}. In 2020, the development of plant activity was delayed due to spreading of the layer of organic material and planting. Thus, LAI was under 0.5 m^2 m^{-2} in June 2020 and reached the largest values (2–2.5 m^2 m^{-2}) only in September–October. In 2021, the largest LAI values (2.5–3.0 m^2 m^{-2}) were observed from June to July. The dry and difficult growing season in 2021 is distinguishable from the very low LAI observations in the nearby agricultural field. The ground level LI-COR LAI measurements produced similar results with the remotely sensed observations. On Sep 1 2020, the average measured LAI was 1.4 m^2 m^{-2} while the remotely sensed LAI was 2.2 m^2 m^{-2}. On Oct 10 2020, the similar LAI values were 2.8 m^2 m^{-2} and 2.3 m^2 m^{-2}, respectively. During summer 2021, the remotely sensed LAI observations were lower on average than the systematic surface observations.

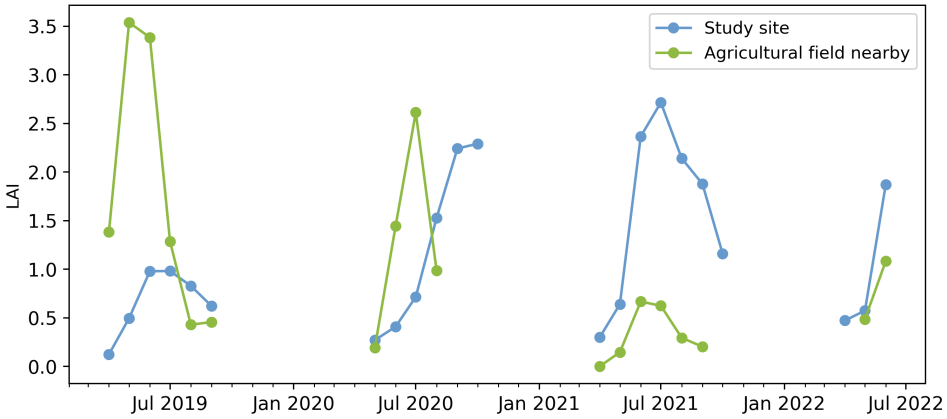

Figure 6: Monthly average leaf area index (LAI) calculated from data retrieved from ESA Sentinel-2 satellites on the study site (blue) and on an agricultural field nearby (green).

DJI Mavic 2 drone (Mavic 2 Pro, SZ DJI Technology Co., Ltd., Shenzhen, China) was used to collect aerial images (e.g. Fig. 1) at the height of 45 m on 1 September 2020, 8 June 2021, and 7 September 2021. OpenDroneMap (WebODM, version 1.9.2) processing software was used to merge the images. Based on the resulting images, it was possible to divide the image pixels into green and non-vegetated parts (using excess green vegetation index ExG=2G-R-B) and thus determine the overall vegetation coverage on the site.

Manual chamber base frames were photographed from above each time the manual chamber measurements were conducted. The photos were first cropped to match the basal area of the base frame and then processed with Canopeo (Patrignani & Ochsner, 2015) to determine the proportion of green area within each base frame (Table 2). Canopeo was used with the default settings. Base frames were situated so that half of them (V1-V3) had vegetation inside them and half of them were bare (B1-B3) in May 2021. Eventually, vegetation developed also within the initially bare base frames and they could no longer be distinguished from the others in that regard in June 2022 (Table 2). The development of green area showed similar seasonal and annual variations than the surface level and remotely sensed LAI observations.

Table 2: Proportion (%) of green area inside the six chamber base frames. In the beginning of the observation period in May 2021, base frames B1, B2, and B3 had no vegetation (B=bare, V=vegetated).

	Green area (%)					
Date	*B1*	*V1*	*B2*	*V2*	*B3*	*V3*
05/2021	0.1	0	0	16	0	15
06/2021	7	3	3	77	1	93
07/2021	35	16	23	75	2	80
08/2021	50	69	48	57	12	25
09/2021	39	91	74	90	23	36
06/2022	90	85	90	80	88	77
07/2022	92	89	96	84	67	72

All tree saplings within each of the sample plots (3×100 m^2) were identified and their heights were measured first in May 2021 and again in July 2022. The results were then upscaled based on the total area of the plots (300 m^2). In May 2021, the densities of spruces and birches were 167 and 267 ha^{-1} with mean height of 22 and 41 cm, respectively. In July 2022, the densities of spruces and birches were 800 and 267 ha^{-1} with mean height of 45 and 142 cm, respectively.

6 JSBACH model setup

The site level simulations were executed with the land surface model JSBACH (Kaminski et al. (2013)), using a version that includes forest management. The soil carbon submodel Yasso (Tuomi et al. (2009)) was utilized to estimate the decomposition of soil organic carbon (SOC).

The JSBACH model was forced with hourly ERA5-Land reanalysis data (Muñoz Sabater (2019)) and ERA5 single level data (Hersbach et al. (2018)) from the grid point nearest to the study site. The simulation spanned over two years from June 2020 to June 2022. The ERA5 forcing data agreed well with the in-situ observed data over the study period (Figure 7).

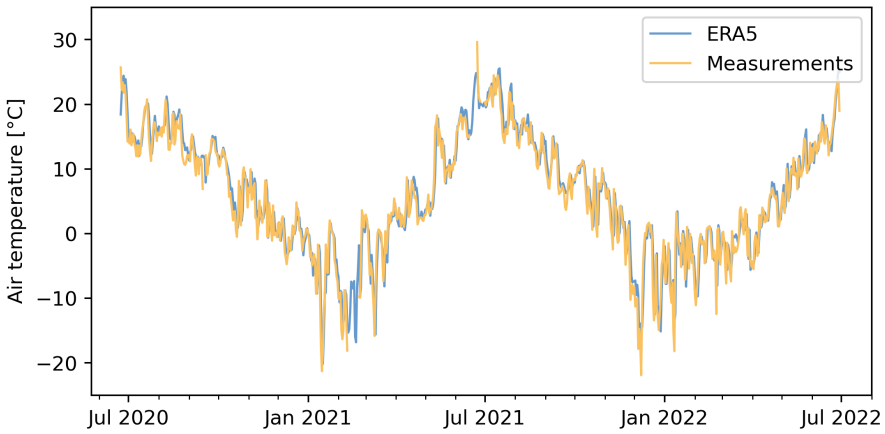

Figure 7: Daily air temperatures compared between ERA5 forcing data and in-situ measurements.

The spin-up and future runs were both forced with EURO-CORDEX data (Jacob et al. (2014)) on the EUR-44 domain, with a spatial resolution of ca. 50 km (0.44 °). The EURO-CORDEX data is downscaled and bias corrected, in this case based on the global driver model CanESM2 under RCP4.5. The model was run with daily EURO-CORDEX from the grid point closest to the study site. Data is available from 1951 to 2100. Additional data was generated for the spin-up by randomly repeating data for 1951 to 1980.

For the study period 2020–2022 the JSBACH model was set to use C3 grass as the plant functional type (PFT), which described the vegetation at the measurement site at the time. The model default parameters were adjusted to represent the conditions at the study site. The maximum leaf area index parameter was set to 4.0 to reproduce the obtained Sentinel-2 satellite LAI observations. Maximum vegetated fraction was set to 0.82 in accordance with the calculated vegetation coverage from the drone imagery. The soil at the site is clay, however, the organic matter spread on top has a very different hydraulic properties. Therefore we used parameter values for field capacity and wilting point based on values representing medium soil texture, which were further tuned using the soil moisture data. The modified JSBACH parameters are listed in Table 3.

Table 3: Parameter settings for JSBACH main simulations.

Parameter (unit)	
Maximum vegetated fraction	0.82
Maximum LAI, grass (m^2 m^{-2})	4.0
Field capacity (%)	40
Wilting point (%)	25

The initial state of the model was derived with a 260-year spin-up run. The spin-up consisted of model runs of 95, 95, and 40 years with vegetation clear-cuts at the end of each period. During the final 30-year spin-up period the leaf area index was limited to zero, in order to bring the model to a new steady state representing the non-vegetated site conditions. The state of the below ground litter pools at the end of the simulation was taken as the initial state for the main run. The above ground litter pools (Table 1)

were initialized at the start of the main run. The bark and woody materials were allocated to the woody AG litter pool whereas sludge was allocated to the green AG litter pool.

A 30-year period was chosen for the future simulations and the JSBACH model was run separately for grass, birch, and spruce vegetation types. In the model PFT setup, these vegetation types were represented by C3 grass, extra-tropical deciduous trees, and extra-tropical evergreen trees, respectively. The initial stem number was 13360 trees ha^{-1} for the reference birch and spruce runs. For the site setup runs, the initial stem numbers were 267 trees ha^{-1} (birch) and 800 trees ha^{-1} (spruce) which were in accordance with the measured densities of the planted birch and spruce seedlings. The given vegetation type was planted in the beginning of each future run and then left to grow for 30 years without any additional disturbances. Then, the annual site CO_2 balance (Fig. 2 in the main publication) was estimated by assuming that the fraction of grass in the area would decrease linearly from 90% to 25%, the fraction of spruce would increase from 5% to 50%, and the fraction of birch would increase from 5% to 25 % in the 30-year time interval. The net ecosystem exchange was calculated as follows: the net primary production (NPP) was calculated as a sum of the NPPs from the spruce model run, birch model run, and the partial (linearly decreasing) grass model run. The site soil respiration was calculated as the weighted average of the grass, birch, and spruce model runs by weighting the proportions as described above. Finally, the estimated site future carbon balance was compared to the reference runs where the vegetation was only grass, dense birch, or dense spruce forest or in a case that there was no vegetation. The non–vegetated future scenario was run with the maximum LAI value set to 0.1.

There are a number of factors contributing to the uncertainty of the carbon sequestrations estimates. Modeling the soil water balance is challenging due to the vertically varying hydraulic properties of the soil layers, clay and added organic material. There is also some uncertainty in assigning the organic material on site to corresponding carbon pools in the JSBACH (Yasso) model. Some of the carbon pools are decomposing very easily and there is no corresponding carbon pool in the model, which is seen in the beginning of the time series as a discrepancy between observed and simulated ecosystem exchange of CO_2 in Fig 1. in the main publication.

References

Chen, T., & Guestrin, C. (2016). Xgboost: A scalable tree boosting system. In *Proceedings of the 22nd acm sigkdd international conference on knowledge discovery and data mining* (pp. 785–794).

Heikkinen, J., Ketoja, E., Seppanen, L., Luostarinen, S., Fritze, H., Pennanen, T., ... Regina, K. (2021). Chemical composition controls the decomposition of organic amendments and influences the microbial community structure in agricultural soils. *Carbon Management*, *12*(4), 359-376. doi: 10.1080/17583004.2021.1947386

Hersbach, H., Bell, B., Berrisford, P., Biavati, G., Horányi, A., Muñoz Sabater, J., ... Thépaut, J.-N. (2018). *Era5 hourly data on single levels from 1959 to present. copernicus climate change service (c3s) climate data store (cds).* (Accessed: 2022-08-05) doi: 10.24381/cds.adbb2d47

Jacob, D., Petersen, J., Eggert, B., Alias, A., Christensen, O. B., Bouwer, L. M., ... Yiou, P. (2014, APR). Euro-cordex: new high-resolution climate change projections for european impact research. *Regional Environmental Change*, *14*(2, SI), 563-578. doi: 10.1007/s10113-013-0499-2

Jokinen, P., Pirinen, P., Kaukoranta, J.-P., Kangas, A., Alenius, P., Eriksson, P., ... Wilkman, S. (2021). *Climatological statistics of Finland 1981–2010.* Meteorological Research and Basic Weather Services, Finnish Meteorological Institute, Helsinki. doi: 10.35614/isbn.9789523361485

Kaminski, T., Knorr, W., Schürmann, G., Scholze, M., Rayner, P., Zaehle, S., ... others (2013). The bethy/jsbach carbon cycle data assimilation system: Experiences and challenges. *Journal of Geophysical Research: Biogeosciences*, *118*(4), 1414–1426. doi: 10.1002/jgrg.20118

Kormann, R., & Meixner, F. (2001). An analytical footprint model for non-neutral stratification. *Boundary-Layer Meteorology*, *99*(2), 207-224. doi: 10.1023/A:1018991015119

Muñoz Sabater, J. (2019). *Era5-land hourly data from 1981 to present. copernicus climate change service (c3s) climate data store (cds).* (Accessed: 2022-08-05) doi: 10.24381/cds.e2161bac

Nevalainen, O., Niemitalo, O., Fer, I., Juntunen, A., Mattila, T., Koskela, O., ... Liski, J. (2022). Towards agricultural soil carbon monitoring, reporting, and verification through the field observatory network (fion). *Geoscientific Instrumentation, Methods and Data Systems*, *11*(1), 93–109.

Patrignani, A., & Ochsner, T. E. (2015). Canopeo: A powerful new tool for measuring fractional green canopy cover. *Agronomy Journal*, *107*(6), 2312–2320.

Tuomi, M., Thum, T., Järvinen, H., Fronzek, S., Berg, B., Harmon, M., ... Liski, J. (2009). Leaf litter decomposition—estimates of global variability based on yasso07 model. *Ecological Modelling*, *220*(23), 3362-3371. doi: https://doi.org/10.1016/j.ecolmodel.2009.05.016

Weiss, M., & Baret, F. (2016). *S2ToolBox Level 2 products: LAI, FAPAR, FCOVER, version 1.1.* `https://step.esa.int/docs/extra/ATBD_S2ToolBox_L2B_V1.1.pdf`.